# Synthesis, characterization, crystal structure and DNA, HSA-binding studies of four Schiff base complexes derived from salicylaldehyde and isopropylamine

Monireh Dehkhodaei, Mahsa Khorshidifard, Hadi Amiri Rudbari, Mehdi Sahihi, Gholamhassan Azimi, Neda Habibi, Salman Taheri, Giuseppe Bruno, Reza Azadbakht

# Synthesis, characterization, crystal structure and DNA, HSA-binding studies of four Schiff base complexes derived from salicylaldehyde and isopropylamine

Monireh Dehkhodaei [a], Mahsa Khorshidifard [a], Hadi Amiri Rudbari [a 1], Mehdi Sahihi [a 1], Gholamhassan Azimi [a], Neda Habibi [b], Salman Taheri [c], Giuseppe Bruno [d], Reza Azadbakht [e]

[a] Department of Chemistry, University of Isfahan, Isfahan 81746-73441, Iran

[b] Department of Biomedical Engineering, College of Engineering, The University of Texas at San Antonio, One UTSA Circle, San Antonio, TX 78249-0619, USA

[c] Chemistry and Chemical Engineering Research Center of Iran, Tehran, Iran

[d] Department of Chemical Sciences, University of Messina, Via F. Stagno d'Alcontres 31, 98166 Messina, Italy

[e] Department of Chemistry, Payame Noor University, P.O. Box 19395-3697, Iran

## Abstract

Four new Schiff base complexes (**$NiL_2$, $CoL_2$, $CuL_2$** and **$ZnL_2$)** (**HL**: ((E)-2-((isopropylamino) methyl) phenol) were synthesized and characterized by CHN elemental analysis, FT-IR and single crystal X-ray diffraction technique. The crystallographic data reveal that in all complexes the metal centers are four-coordinated by two phenolate oxygen and two imine nitrogen atoms of two moles of Schiff base ligand **HL** and geometry around the metal center in all of them is distorted tetrahedral. In addition, $^{1}H$ and $^{13}C$ NMR techniques were employed for characterization of diamagnetic **$ZnL_2$** complex. The binding affinity of complexes with DNA (fish sperm DNA, FS-DNA) and Human Serum Albumin (HSA) were investigated using fluorescence quenching, chemometrics, UV–Vis spectroscopy, viscosity measurements and molecular docking methods. The obtained results revealed that the DNA and HSA affinity for binding to complexes are in the following order: **$CuL_2$** > **$ZnL_2$** > **$CoL_2$** > **$NiL_2$** and **$NiL_2$** > **$ZnL_2$** > **$CuL_2$** > **$CoL_2$**. The distance between complexes and HSA was obtained based on the Förster's theory of non-radiative energy transfer. The computational molecular docking results showed that H-bond interactions, hydrophobic interactions, π-π stacking and π-cation interactions have dominant role in the stability of HSA-**$ML_2$** (M: Cu, Co, Ni and Zn). The computational docking and viscosity results suggest that all metal complexes interact with DNA presumably by the groove binding mechanism.

## Keywords

DNA interaction

HSA binding

Schiff base complex

Crystal structure

## 1. Introduction

The medicinal properties of transition metal complexes depend on both the nature of the ligands and metal ions [1]. Schiff base ligands have attracted great interest because of their broad range of biological as well as pharmaceutical properties such as antibacterial, antioxidant, anti-malarial and antitumor activities [2], [3], [4], [5], [6], [7], [8], [9], [10], [11], [12], [13]. The azomethine linkage in Schiff base is responsible antimicrobial activity. Presence of lone pair electrons in $sp^2$-hybridized orbital of nitrogen atom in the azomethine group plays a remarkable chemical and biological role [14], [15]. Among the Schiff base ligands, bidentate and tetradentate Schiff base ligands involving N,O donor sites possess many advantages such as facile synthesis, readily adjusted ancillary ligands, and tunable steric and electronic coordination environments on the metal center. These complexes represent interesting models for metallo-enzymes which efficiently catalyze the reduction of dinitrogen and dioxygen [16], [17], [18], [19].

The metal ion of the complexes accelerates the drug activity and increases the effectiveness and efficiency of the ligands [20]. In recent decades, considerable effort has been devoted to the design and development of complexes by using different metal ions, which possess excellent antioxidant, antibacterial and antitumor activities. Investigations showed that metal ions such as cobalt, nickel, copper and zinc could have remarkable biological activity [21], [22], [23], [24], [25], [26], [27], [28], [29].

Previously, we have reported the bi-dentate ON Schiff base ligand derived from condensation of isopropylamine with salicylaldehyde (**HL)** and its oxovanadium(IV) complexes [30]. Continuing of our research in design of new Schiff base ligands, complexes [31], [32], [33], [34], [35], [36], [37], [38], [39], [40], [41], [42], [43], [44], [45] and their interaction with bio macromolecules, herein we present the results of a detailed investigation on the HSA and DNA interaction of new distorted tetrahedral complexes, **$NiL_2$, $CoL_2$, $CuL_2$** and **$ZnL_2$**, derived from **HL** ligand. The new complexes have been characterized by IR, elemental analysis and single-crystal X-ray diffraction. The $^1H$ and $^{13}C$ NMR techniques were employed for characterization of the **$ZnL_2$** complex. The HSA and DNA binding affinity of complexes were investigated by using fluorescence quenching, chemometrics, UV–Vis spectroscopy, viscosity measurements as well as molecular docking methods.

## 2. Experimental section

### 2.1. Chemicals and instrumentation

Fish sperm DNA (FS-DNA), human serum albumin (HSA) and ethidium bromide (3,8-diamino-5-ethyl-6-phenylphenanthridinium bromide, EtBr) were purchased from Sigma-Aldrich. Other chemicals were purchased from Merck Co. and used without further purification. The FT-IR spectra were recorded on a JASCO, FT-IR 6300 spectrometer (4000–400 $cm^{-1}$) in KBr pellets. $^1H$ and $^{13}C$ NMR spectra of Zn(II) complexes were recorded on a Bruker Avance 400 spectrometer using deuterated chloroform ($CDCl_3$) as solvents. Elemental analysis was performed on Leco, CHNS-932 and Perkin-Elmer 7300 DV elemental analyzers. UV–Vis spectra were recorded on a JASCO V-670 spectrophotometer. Fluorescence and Viscosity measurements were carried out at room temperature using Shimadzu RF-5000 spectrofluorometer and a Brookfield rotational viscometer, respectively.

## 2.2. Preparation of complexes

### *2.2.1. General procedures*

A MeOH solution (30 mL) of isopropylamine (5 mmol) was added dropwise to a MeOH solution (30 mL) of the salicylaldehyde (5 mmol), stirred for 2 h at ambient temperature (yellow solution A). Triethylamine (7 mmol) in MeOH (10 mL) was added to yellow solution A and stirred for 10 min with formation of a dark yellow solution (solution B). A solution of $NiCl_2 \cdot 6H_2O$, $Co(NO_3)_2 \cdot 6H_2O$, $Cu(OAc)_2$ or $Zn(NO_3)_2 \cdot 6H_2O$, (2.5 mmol) in MeOH (30 mL) was added drop wise to solution B.

### *2.2.2. Cobalt(II) complex (CoL$_2$)*

An immediate precipitation of **CoL$_2$** complex occurred on addition of $Co(NO_3)_2 \cdot 6H_2O$ to solution B. The reaction mixture was stirred for 8 h in ambient temperature and orange precipitates were collected by filtration, washed with cold methanol, and dried in air with a typical yield of 82%. Orange crystals suitable for single crystal X-ray diffraction analysis were obtained from the filtrate standing for 2 days at room temperature. Anal. calc. for $C_{20}H_{24}CoN_2O_2$: C: 62.66, H: 6.31, N: 7.31.

Found: C: 62.69, H: 6.36, N: 7.28. Selected IR data (KBr, $cm^{-1}$): 3058–2867 ($\nu_{C\ \ N}$), 1605 ($\nu_{C\ \ N}$), 1536 ($\nu_{C\ \ C}$), 1143 ($\nu_{C\text{-}O}$).

### *2.2.3. Nickel(II) complex (NiL$_2$)*

An immediate precipitation of **NiL$_2$** complex occurred on addition of $NiCl_2 \cdot 6H_2O$ to solution B. The reaction mixture was stirred for 8 h in ambient temperature and green precipitates were collected by filtration, washed with cold methanol, and dried in air with a typical yield of 82%. Green crystals suitable for single crystal X-ray diffraction analysis were collected from the filtrate standing for 2 days at room temperature. Anal. calc. for $C_{20}H_{24}NiN_2O_2$: C: 62.70, H: 6.31, N: 7.31.

Found: C: 62.75, H: 6.27, N: 7.30. Selected IR data (KBr, $cm^{-1}$): 3051–2864 ($\nu_{C\ \ N}$), 1609 ($\nu_{C\ \ N}$), 1536 ($\nu_{C\ \ C}$), 1142 ($\nu_{C\text{-}O}$).

### *2.2.4. Copper(II) complex (CuL$_2$)*

A red solution was obtained on addition of $Cu(OAc)_2$ to solution B. The reaction mixture stirred for 8 h at ambient temperature and allowed to stand overnight. Big red crystals were collected by filtration with a typical yield of 91%. Appropriate single crystals for X-ray crystallography were obtained directly from the reaction mixture. Anal. calc. for $C_{20}H_{24}CuN_2O_2$: C: 61.92, H: 6.24, N: 7.22. Found: C: 61.87, H: 6.30, N: 7.23. Selected IR data (KBr, $cm^{-1}$): 3045–2857 ($\nu_{C\ \ N}$), 1614 ($\nu_{C\ \ N}$), 1536 ($\nu_{C\ \ C}$), 1143 ($\nu_{C\text{-}O}$).

### *2.2.5. Zinc(II) complex (ZnL$_2$)*

A yellow solution was obtained on addition of $Zn(NO_3)_2 \cdot 6H_2O$ to solution B. The reaction mixture refluxed for 8 h and slowly evaporated to dryness at room temperature. The yellow solid was purified by washing with diethyl ether (50 mL) and dried in air with a typical yield of 85%. Appropriate single crystals for X-ray crystallography were obtained directly from the reaction mixture. Anal. calc. for $C_{20}H_{24}N_2O_2Zn$: C: 61.62, H: 6.21, N: 7.19. Found: C: 61.59, H: 6.25, N:

7.23. Selected IR data (KBr, $cm^{-1}$): 3051–2896 ($\nu_{C\ \ N}$), 1617 ($\nu_{C\ \ N}$), 1539 ($\nu_{C\ \ C}$), 1144 ($\nu_{C\text{-}O}$). $^{1}$HNMR and $^{13}$CNMR (DMSO-$d_6$, 400 MHz, 298 K): Table 3.

Table 1. Crystal data and structure refinement.

| Empty Cell | **$CoL_2$** | **$NiL_2$** | **$CuL_2$** | **$ZnL_2$** |
|---|---|---|---|---|
| Empirical formula | $C_{20}H_{24}N_2O_2Co$ | $C_{20}H_{24}N_2O_2Ni$ | $C_{20}H_{24}N_2O_2Cu$ | $C_{20}H_{24}N_2O_2Zn$ |
| Formula weight | 383.34 | 383.12 | 387.95 | 389.78 |
| Temperature (K) | 298(2) K | 298(2) K | 298(2) K | 298(2) K |
| Wavelength (Å) | 0.71073 Å | 0.71073 Å | 0.71073 Å | 0.71073 Å |
| Crystal system | Orthorhombic | Orthorhombic | Orthorhombic | Orthorhombic |
| Space group | *Pbca* | *Pbca* | *Pbca* | *Pbca* |
| *Unit cell dimensions* | | | | |
| a(Å) | 15.197(5) | 15.1077(4) | 14.698(3) | 15.1429(5) |
| b(Å) | 13.200(5) | 13.1296(4) | 12.918(3) | 13.2248(4) |
| c(Å) | 19.427(5) | 19.6231(6) | 20.898(4) | 19.4834(7) |
| *β (°)* | | | | |
| Volume ($Å^3$) | 3897(2) | 3892.4(2) | 3967.9(14) | 3901.8(2) |
| Z | 8 | 8 | 8 | 8 |
| Density (calculated) ($Mg/m^3$) | 1.307 | 1.308 | 1.299 | 1.327 |
| Absorption coefficient ($mm^{-1}$) | 0.895 | 1.011 | 1.115 | 1.273 |
| F(000) | 1608 | 1616 | 1624 | 1632 |

| Empty Cell | **$CoL_2$** | **$NiL_2$** | **$CuL_2$** | **$ZnL_2$** |
|---|---|---|---|---|
| Theta range for data collection (°) | 2.10 to 25.00 | 2.30 to 26.99 | 2.39 to 25.00 | 2.09 to 29.90 |
| Index ranges | $-18 \le h \le 18$ | $-19 \le h \le 19$ | $-15 \le h \le 12$ | $-18 \le h \le 21$ |
| | $-15 \le k \le 14$ | $-16 \le k \le 16$ | $-14 \le k \le 11$ | $-18 \le k \le 17$ |
| | $-23 \le l \le 23$ | $-21 \le l \le 25$ | $-24 \le l \le 12$ | $-27 \le l \le 26$ |
| Reflections collected | 53364 | 30086 | 16410 | 38722 |
| Independent reflections | 3429 [$R_{(int)} = 0.0367$] | 4245 [$R_{(int)} = 0.0243$] | 3187 [$R_{(int)} = 0.0556$] | 5636 [$R_{(int)} = 0.0303$] |
| Data Completeness (%) | 99.6% | 100% | 91.3% | 99.8% |
| Refinement method | Full-matrix least-squares on $F^2$ | Full-matrix least-squares on $F^2$ | Full-matrix least-squares on $F^2$ | Full-matrix least-squares on $F^2$ |
| Data/restraints/parameters | 3429/0/226 | 4245/0/226 | 3187/0/226 | 5636/0/226 |
| Goodness-of-fit on $F^2$ | 1.170 | 1.094 | 1.046 | 1.103 |
| Final R indices [$I > 2\sigma(I)$] | $R_1 = 0.0312$ | $R_1 = 0.0327$ | $R_1 = 0.0444$ | $R_1 = 0.0394$ |
| | $wR_2 = 0.0830$ | $wR_2 = 0.0815$ | $wR_2 = 0.1097$ | $wR_2 = 0.0913$ |
| R indices (all data) | $R_1 = 0.0413$ | $R_1 = 0.0443$ | $R_1 = 0.0664$ | $R_1 = 0.0647$ |
| | $wR_2 = 0.0921$ | $wR_2 = 0.0899$ | $wR_2 = 0.1241$ | $wR_2 = 0.1057$ |
| Largest diff. peak and hole ($e.Å^{-3}$) | 0.263 and −0.380 | 0.268 and −0.269 | 0.558 and −0.725 | 0.429 and −0.375 |

Table 2. Selected bond distances (Å) and angles **(°) for $CoL_2$, $NiL_2$, $CuL_2$ and $ZnL_2$.**

| Empty Cell | **$CoL_2$** | **$NiL_2$** | **$CuL_2$** | **$ZnL_2$** |
|---|---|---|---|---|
| M(1)—O(1) | 1.9050(15) | 1.8943(15) | 1.902(2) | 1.9098(16) |

| Empty Cell | **$CoL_2$** | **$NiL_2$** | **$CuL_2$** | **$ZnL_2$** |
|---|---|---|---|---|
| M(1)—O(2) | 1.9117(15) | 1.8879(14) | 1.900(2) | 1.9205(16) |
| M(1)—N(1) | 2.0004(17) | 1.9768(17) | 1.993(3) | 2.0110(16) |
| M(1)—N(2) | 1.9896(18) | 1.9840(16) | 1.998(3) | 2.0028(18) |
| N(1)—C(7) | 1.288(2) | 1.282(3) | 1.298(4) | 1.287(3) |
| N(2)—C(17) | 1.284(3) | 1.288(2) | 1.284(5) | 1.282(3) |
| O(1)-M(1)-O(2) | 118.48(7) | 125.09(7) | 137.55(11) | 117.25(7) |
| N(1)-M(1)-N(2) | 122.51(7) | 120.61(7) | 137.70(13) | 122.62(7) |
| O(1)-M(1)-N(1) | 96.37(6) | 94.21(7) | 94.56(10) | 96.84(7) |
| O(1)-M(1)-N(2) | 112.06(7) | 112.89(7) | 99.78(12) | 112.27(8) |
| O(2)-M(1)-N(1) | 112.79(7) | 112.26(7) | 100.98(11) | 112.71(7) |
| O(2)-M(1)-N(2) | 96.31(7) | 94.15(6) | 94.74(12) | 96.64(7) |

Table 3. $^{1}$H NMR and $^{13}$C NMR data for **$ZnL_2$**.

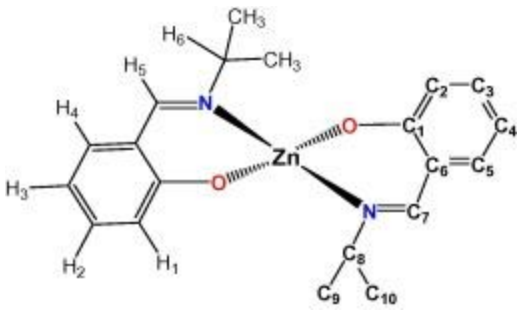


| Empty Cell | **$^{1}$HNMR** | Empty Cell | **$^{13}$CNMR** |
|---|---|---|---|
| $H_1$ | 6.86 (d) | $C_1$ | 170.3 |
| $H_2$ | 7.31 (d of t) | $C_2$ | 114.3 |
| $H_3$ | 6.60 (d of t) | $C_3$ | 135.7 |
| $H_4$ | 7.11 (d of d) | $C_4$ | 123.1 |
| $H_5$ | 8.24 (s) | $C_5$ | 134.9 |
| $H_6$ | 3.64 (septet) | $C_6$ | 118.0 |
| $CH_3$ | 1.22 (d) and 1.32 (d) | $C_7$ | 169.1 |
| | | $C_8$ | 62.6 |
| | | $C_9$, $C_{10}$ | 24.3 and 23.9 |

s, singlet; d, doublet; t, triplet.

### 2.3. Single crystal diffraction studies

The X-ray data of complexes (**NiL$_2$, CoL$_2$, CuL$_2$** and **ZnL$_2$**) were collected at room temperature with a Bruker APEX II CCD area detector diffractometer using Mo Kα radiation (λ = 0.71073 Å). Data collections, cell refinements, data reductions and absorption corrections were performed using multiscan methods with Bruker software [46]. The structures were solved by direct methods using SIR2004 [47]. The non-hydrogen atoms were refined anisotropically by the full matrix least squares method on $F^2$ using SHELXL [48]. All hydrogen atoms were added at ideal positions and constrained to ride on their parent atoms. Molecular graphics were prepared with the Olex2 program [49]. Crystallographic data for complexes are listed in Table 1. Selected bond distances and angles are summarized in Table 2.

## 2.4. DNA binding studies

### *2.4.1. Preparation of compounds and DNA stock solutions*

The stock solution of FS-DNA was prepared by 50 mM Tris buffer at pH 7.5 using double-distilled deionized water and stored at 4 °C. The FS-DNA concentration per nucleotide was determined using absorption intensity at 260 nm after adequate dilution with the buffer and using the reported molar absorptivity of 6600 $M^{-1}.cm^{-1}$ [50]. Purity of FS-DNA solution was confirmed by ratio of UV absorbance at 260 and 280 nm ($A_{260}/A_{280}$ = 1.9), indicating that FS-DNA is free from protein impurity [51]. The complex solutions in methanol as co-solvent were diluted with corresponding buffer to the required concentration for all experiments. The volume of co-solvent never exceeded 5% (v/v), so the effect of methanol is negligible. To confirm the stability of the metal complexes in the buffer solution at room temperature, a UV–Vis study was performed. The spectral features of the complexes exhibited no change in the position of absorption bands over a period of 24 h and no precipitation or turbidity was observed even after long storage at room temperature (at least 1 month after preparation). This indicates the stability of the compounds in different media. However, all the solutions were used freshly after preparation.

### *2.4.2. UV–Vis spectroscopy measurements*

Absorption titration experiment as an operational and very easy method was carried out to investigate of DNA-binding of the compounds at room temperature. Absorption spectral titration experiments were performed by addition of various amounts of DNA ($0–5 \times 10^{-4}$ M) to the compounds ($1 \times 10^{-4}$ M). All compounds–DNA solutions were allowed to incubate for 2 min before recording the related spectra. Absorption curves of compounds–DNA mixtures were corrected by subtracting the spectra of DNA and all intensities were corrected for the dilution effect.

### *2.4.3. Fluorescence spectroscopic measurements*

Fluorescence quenching experiments was carried out using quartz cuvette with 1 cm optical path length and the excitation and emission slits were set at 5 and 10 nm, respectively. In our primary experiments, ethidium bromide (EtBr) emission was checked in the presence of various amounts of DNA. The results showed that the emission of EtBr was increased up to DNA:EtBr = 10:1 mol ratio and there was no significant increasing in emission after the mentioned mole ratio. The FS-DNA solution was stirred with EtBr with molar ratio of DNA:EtBr 10:1 and incubated for 1 h at 4 °C to completion of interaction between DNA and EtBr. Various amounts of metal complexes (0–250 μM) were added to the mixture of DNA:EtBr. The fluorescence spectra were measured in the range of 500–700 nm with exciting wavelength at 520 nm. In each measurement after addition of metal complexes, the mixture was allowed to stand for 2 min. Moreover, the measured fluorescence intensities were corrected for the dilution and the inner-filter effect. To eliminate the inner filter effects, absorption measurements were carried out at the fluorescence excitation and emission wavelengths. The extent of this effect can be roughly evaluated with the following relationship [52]:

$$F_{corr} = F_{obs} \times e^{(A_{ex}+A_{em})/2} \quad (1)$$

Where $F_{corr}$ and $F_{obs}$ are the corrected and observed fluorescence intensities, respectively, while $A_{ex}$ and $A_{em}$ are the absorption of compounds at excitation and emission wavelengths, respectively. It was assumed that fluorescence spectra of solutions with low concentration ($A_{FL}$ = 0.1) are not disturbed by reabsorption effect [53].

#### *2.4.4. Viscosity measurements*

Viscosity experiments were carried out using a rotational viscometer and the measurements were performed at 200 rpm at room temperature. The viscosity of DNA solution was measured in the presence of increasing amounts of the metal complexes. The obtained data are presented as $(\eta/\eta_0)^{1/3}$ versus [complex]/[DNA], where $\eta_0$ and $\eta$ are the viscosity of DNA in the absence and presence of the metal complexes, respectively.

### 2.5. HSA binding experiments

#### *2.5.1. Preparation of protein stock solution*

A stock solution of HSA was prepared by dissolving the desired amount of HSA in 50 mM phosphate buffer (pH = 7). The HSA stock solution was stored at 4 °C in the dark and used within 2 h. HSA concentration was determined by UV–Vis spectrophotometry using the molar absorption coefficient 35700 $M^{-1}.cm^{-1}$ at 278 nm [54].

#### *2.5.2. Fluorescence spectroscopic measurements*

The interaction of HSA with the synthesized Schiff base complexes (**$ZnL_2$**, **$CuL_2$**, **$NiL_2$** and **$CoL_2$**) was investigated using fluorescence quenching experiment. In this experiment 2 mL of HSA solution (5 µM) was placed into the cell and various amounts of the compounds (0–50 µM) were added to the cell. The fluorescence intensity was measured with investigation of excitation wavelength at 295 nm and emission wavelength range of 300–450 nm. In each measurement, the mixture was allowed to incubate for 2 min after addition of the complexes. All intensities were corrected for the dilution and inner filter effect in fluorescence experiments.

#### *2.5.3. UV–Vis absorption measurements*

Absorption titration experiment as an operational and very easy method was also carried out to investigate the HSA binding of complexes at room temperature. The UV–Vis absorption spectra of the complexes solution (10 µM) in the absence and presence of various amounts of the HSA (0–50 µM) were recorded. Absorption curves of compounds–protein mixtures were corrected by subtracting of HSA solution spectra.

### 2.6. Molecular docking simulation

In this work, docking study was carried out to indicate DNA and HSA binding site for the synthesized compounds. The 3D structures of the metal complexes were generated using the CIF files of their X-ray crystal structures. The CIF files were converted to the PDB format by using the Mercury software (http://www.ccdc.cam.ac.uk/). The known crystal structures of DNA (PDB

ID: 423D) with sequence d(ACCGACGTCGGT)$_2$ and HSA (PDB ID: 1AO6) were taken from the Brookhaven Protein Data Bank (http://www.rcsb.org/pdb). The resolution of these files was 0.160 and 0.25 Å for DNA and HSA, respectively. Water molecules of the PDB files were removed and missing hydrogen atoms were added. Flexible-ligand docking was performed by AutoDock 4.2.5.1 molecular-docking program using the implemented empirical free energy function and the Lamarckian Genetic Algorithm [55]. The Gasteiger charges were added to prepare the macromolecule input file for docking and the Auto Grid was used to calculate Grids. A blind docking with 126 lattice points along X, Y, and Z axes was performed for docking of metal complexes with DNA to find the binding site of complexes on DNA with a grid point spacing of 0.375 Å and to allow the complex to rotate freely. The Center of the grid box was located at the binding site and the second docking was performed using a cubic box with $60 \times 60 \times 60$ dimensions. For the docking of synthesized metal complexes to HSA the grid box was centred on $C_\alpha$ of Trp-214 residue and a docking with 90 lattice points along X, Y, and Z axes was performed to find the binding site of complexes on HSA. 250 docking runs with 25,000,000 energy evaluations for each run were performed.

## 3. Results and discussion

### 3.1. Synthesis and spectroscopic characterization of the complexes

The reaction of Schiff base ligand with metal ions is shown in Scheme 1. All of complexes were obtained in good yield (more than 80%). The elemental analyses of the complexes were consistent with their proposed compositions. These results are also confirmed by X-ray crystallography. Stability of all complexes in the most common polar and non-polar solvents including $H_2O$, MeOH, EtOH, $CH_3CN$, $CHCl_3$, DMSO and DMF was tested and the results showed the stability of complexes in solvents.

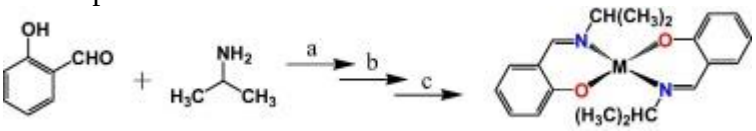


Scheme 1. Synthetic routes for the preparation of the complexes: (a) stirring of isopropylamine and salicylaldehyde in MeOH at ambient temperature; (b) adding of trimethylamine to solution and stirring for 10 min; (c) adding of metal salt $MX_2$ and stirring in ambient temperature for Co(II), Ni(II) and Cu(II); for Zn(II) complex in reflux condition ($MX_2$: $NiCl_2{\cdot}6H_2O$, $Co(NO_3)_2{\cdot}6H_2O$, $Cu(OAc)_2$, $Zn(NO_3)_2{\cdot}6H_2O$).

The most characteristic feature in the IR spectra of the metal complexes comes from the C N stretching vibrations. This band appeared at 1605, 1609, 1614 and 1617 $cm^{-1}$ for the cobalt(II), nickel(II), copper(II), zinc(II) complexes, respectively [31], [32], [34]. Compared to the free Schiff base ligand (**HL**) (1630 $cm^{-1}$) [30], this band was shifted to lower wavenumber upon coordination. Formation of M-N bonds leads to weakening of C N band and this can be explained by the donation of electrons from the nitrogen atom to the empty orbitals of the metal atom. The presence of several medium intensity bands between 3051–2857 $cm^{-1}$ suggests the existence of C H stretching vibrations of aliphatic and aromatic protons. The C O stretching vibration, 1143 $cm^{-1}$ (**CoL$_2$** and **CuL$_2$**), 1142 $cm^{-1}$ (**NiL$_2$**) and

1144 $cm^{-1}$ for **$ZnL_2$,** confirms the presence of phenolate group in the complexes. Additional support for the formation of the complexes were provided by the existence of weak intensity bands at ~480 $cm^{-1}$ attributed to the formation of M-N and M-O bonds.
The diamagnetic zinc(II) complex, **$ZnL_2$** was studied by $^1H$ and $^{13}C$ NMR experiments (Table 3). The $^1H$ and $^{13}C$ NMR spectra of **$ZnL_2$** complex showed the expected simple spectra, indicating the integrity of the complex. The spectra of **$ZnL_2$** complex obtained after 12, 24 and 120 h were similar to the initial spectrum, indicating that the complex is stable in deuterated chloroform. The signal for the imine proton in the zinc(II) complex appears at 8.24 ppm. This signal shifted downfield with respect to the corresponding signal in the free ligand (8.36 ppm), which is consistent with the coordination of the azomethine nitrogen atom to the metal ion and also indicates that the metal-nitrogen bond is retained in solution. Also, $^1H$ NMR spectrum shows the hydrogens of methyl group as two doublets at 1.22 and 1.32 ppm and methine protons as one septet at 3.64 ppm. The protons of each $CH_3$ group give different signal in $^1H$ NMR spectrum (Table 3) and confirms that protons of each $CH_3$ group are in different chemical environments in **$ZnL_2$** complex. The splitting reason of CH and $CH_3$ peaks is the coupling of hydrogens of CH and $CH_3$ with together.
No signal corresponded to hydroxyl proton at 13.7 ppm and this suggested that the hydroxyl group was fully deprotonated and the oxygen was most likely coordinated to the metal ion. The $^{13}C$ NMR spectrum of **$ZnL_2$** complex show 10 signals. The peak at 169.1 ppm in $^{13}C$ NMR spectrum of **$ZnL_2$** assignable to the imine carbon atoms, confirms the presence of the Schiff base ligand in the complex [34], [45]. The results shown in Table 3 confirmed that carbons of two $CH_3$ groups are in different chemical environments (24.3 and 23.9 ppm) and that they appeared as two signals in $^{13}C$ NMR spectrum.

### 3.2. Description of the crystal structures

View of the molecular structures of **$NiL_2$, $CoL_2$, $CuL_2$** and **$ZnL_2$** complexes with common atom numbering scheme are shown in Fig. 1, Fig. 2, Fig. 3, Fig. 4, respectively. The crystallographic data and selected bond lengths and angles are collected in Table 1, Table 2, respectively. The crystallographic data reveal that in all complexes the metal center is four coordinated by two phenolate oxygen and two imine nitrogen atoms of two moles of Schiff base ligand **HL**. The geometry around the metal center in all complexes is distorted tetrahedral [32]. The C N bond distances are 1.288(2) (N1 = C7) and 1.284(3) Å (N2 = C18) for **$CoL_2$**, 1.282(3) (N1 = C7) and 1.288(2) Å (N2 = C18) for **$NiL_2$**, 1.298(4) (N1 = C7) and 1.284(5) Å (N2 = C18) for **$CuL_2$** and 1.287(3) (N1 = C7) and 1.282(3) Å (N2 = C18) for **$ZnL_2$** consistent with the C N bond when coordinated to a metal center [32].

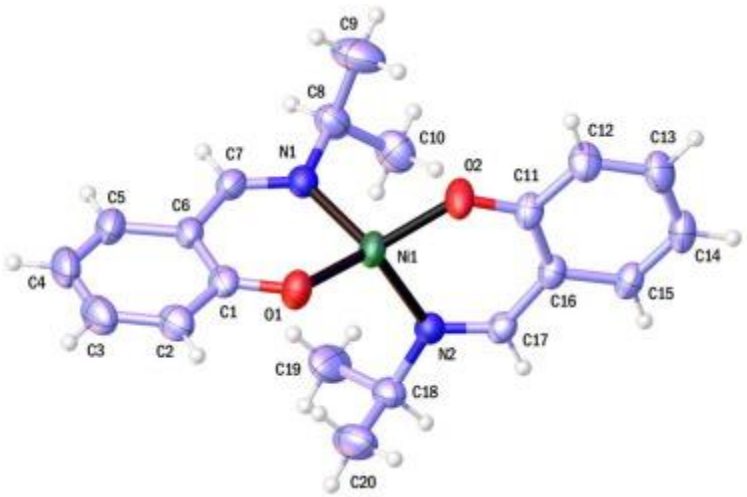


Fig. 1. ORTEP representation of **NiL**$_2$. Displacement ellipsoids are drawn at the 30% probability level and H atoms are shown as small spheres of arbitrary radii.

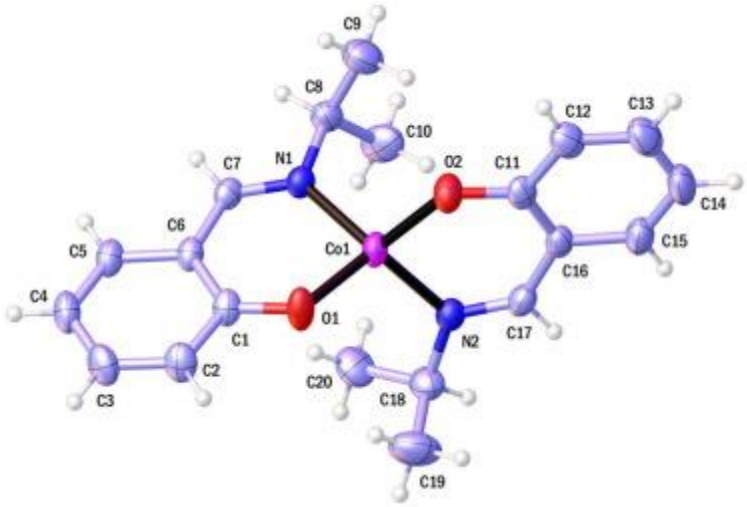


Fig. 2. ORTEP representation of **CoL**$_2$. Displacement ellipsoids are drawn at the 30% probability level and H atoms are shown as small spheres of arbitrary radii.

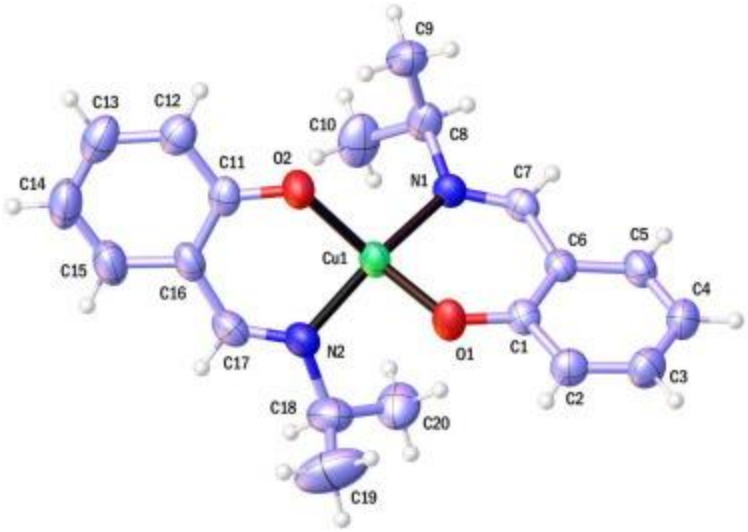


Fig. 3. ORTEP representation of **CuL**$_2$. Displacement ellipsoids are drawn at the 30% probability level and H atoms are shown as small spheres of arbitrary radii.

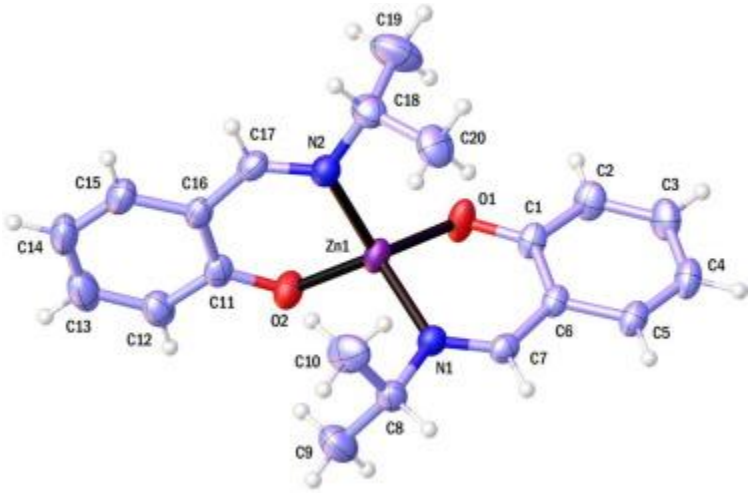


Fig. 4. ORTEP representation of **ZnL**$_2$. Displacement ellipsoids are drawn at the 30% probability level and H atoms are shown as small spheres of arbitrary radii.

Examination of the main metal-ligand distances shows that the M—N distances are longer than the M—O distances due to stronger ability of the oxygen atom to bond to the metal than the nitrogen atom. The M—N distances are 2.0004(17) and 1.9896(18) Å for **CoL**$_2$, 1.9768(17) and 1.9840(16) Å for **NiL**$_2$, 1.993(3) and 1.998(3) Å for **CuL**$_2$ and 2.0110(16) and 2.0028(18) Å for **ZnL**$_2$. While, the M—O distances are 1.9050(15) and 1.9117(15) Å for **CoL**$_2$, 1.8943(15) and 1.8879(14) Å for **NiL**$_2$, 1.902(2) and 1.900(2) Å for **CuL**$_2$ and 1.9098(16) and 1.9205(16) Å for **ZnL**$_2$. The N(1)–M–N(2) angle in **CuL**$_2$ is larger than the other complexes (122.51(7)° for **CoL**$_2$; 120.61(7)° for **NiL**$_2$; 137.70(13)° for **CuL**$_2$ and 122.62(7)° for **ZnL**$_2$). With such an angle in **CuL**$_2$, the distance and steric hindrance between the two isopropyl groups in **CuL**$_2$ are greater and lower respectively than other complexes.

Structures of Cobalt(II), Copper(II), Zinc(II) and Palladium(II) Schiff base complexes, **CoL′**$_2$, **CuL′**$_2$, **ZnL′**$_2$ and **PdL′**$_2$ derived from salicylaldehyde and tert-butylamine

have been previously reported by our group [32]. The crystal structure of theses complexes also show a distorted tetrahedral geometry around the metal center. There was no structural change in the complexes by changing the tert-butylamine to isopropylamine, except some change in distances and angles (Fig. 5). The most important change is the M-N bond lengths in two types of complexes (Fig. 5). The M-N bond lengths in complexes derived from salicylaldehyde and isopropylamine (**CoL$_2$**, **CuL$_2$** and **ZnL$_2$**) are shorter than complexes derived from salicylaldehyde and tert-butylamine (**CoL′$_2$**, **CuL′$_2$** and **ZnL′$_2$**) (Fig. 5). The steric hindrance of ancillary groups on nitrogen atom of azomethine group (tert-butyl or isopropyl) are responsible in increase or decrease of M-N bond lengths. For example see comparison between **CuL$_2$** and **CuL′$_2$** complexes in Fig. 6. The X-ray results showed that the hydrogen atoms of two tert-butyl group coordinated to metal center in **CoL′$_2$**, **CuL′$_2$** and **ZnL′$_2$** complexes have higher steric crowding than hydrogen atoms of two isopropyl group in **CoL$_2$**, **CuL$_2$** and **ZnL$_2$** complexes (Fig. 6). This steric hindrance reduced the M-N bond lengths in **CoL′$_2$**, **CuL′$_2$** and **ZnL′$_2$** and increased the M-N bond lengths in **CoL$_2$**, **CuL$_2$** and **ZnL$_2$**.

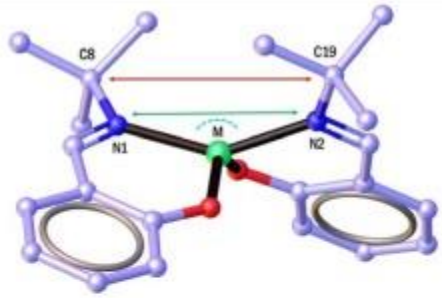


| | $d_{N1-N2}$ | $d_{C8-C19}$ | $\alpha_{N1-M-N2}$ |
|---|---|---|---|
| **CoL′$_2$** | 3.506(5) | 4.875(5) | 122.03(12) |
| **CuL′$_2$** | 3.795(4) | 5.358(5) | 145.58(8) |
| **ZnL′$_2$** | 3.609(3) | 5.025(4) | 126.95(13) |

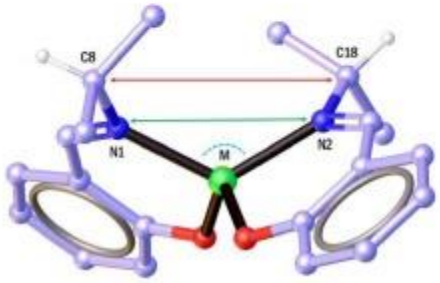


| | $d_{N1-N2}$ | $d_{C8-C18}$ | $\alpha_{N1-M-N2}$ |
|---|---|---|---|
| **CoL$_2$** | 3.498(3) | 4.989(4) | 122.52(7) |
| **CuL$_2$** | 3.722(4) | 5.479(6) | 137.69(11) |
| **ZnL$_2$** | 3.521(2) | 5.023(3) | 122.63(7) |
| **NiL$_2$** | 3.441(2) | 4.913(3) | 120.61(17) |

Fig. 5. Distances (Å) and angles (°) between the two butyl groups in the **CoL′$_2$**, **CuL′$_2$** and **Zn′L$_2$** complexes (Ref. 32) and between the two isopropyl groups in the **CoL$_2$**, **CuL$_2$**, **ZnL$_2$** and **NiL$_2$** (this work).

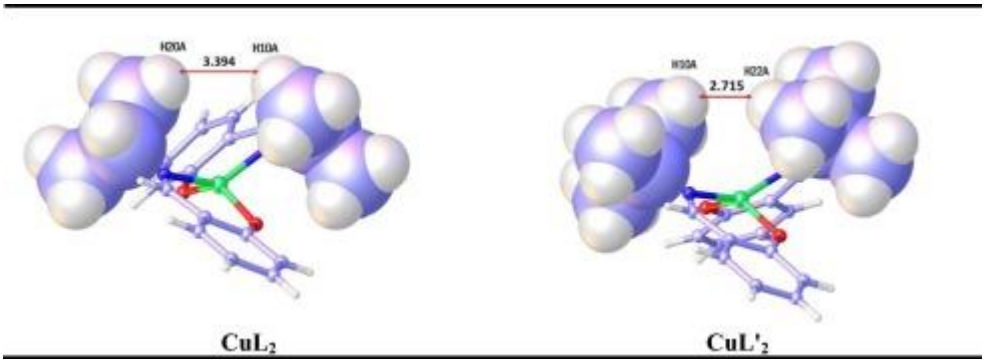


Fig. 6. Steric hindrance of hydrogen atoms in **CuL$_2$** and **CuL′$_2$** complexes.

### 3.3. Interaction with DNA

#### *3.3.1. UV–Vis absorption*

UV–Vis spectroscopy is an effective method to obtain valuable information about binding mode and binding affinity of various types of compounds to biomacromolecules [56]. Generally, hyperchromic or hypochromic effect and red or blue shift are observed in the UV–vis spectrum of a drug upon its DNA-binding. Both hypochromic and red shift are indicative of intercalation mode involving an interaction between π∗-orbital of drug with π-orbital of DNA base pairs. Therefore, energy level of π∗-orbital of drug decreases which causes red shift in its UV–vis spectrum. Furthermore, the coupled π∗-orbital is filled and so the probability of electron transition decreased and hypochromic is observed. While a groove binding or electrostatic interaction leads to hyperchromic effect along with blue shift. A hyperchromic effect can be due to breakage of the secondary structure of DNA [57], [58]. The absorption spectra of the synthesized metal complexes both in the absence and presence of different concentrations of FS-DNA were given in Figs. 7 and S1. The intensity of these spectra decreased with the addition of FS-DNA. To quantitatively evaluate the affinity of compounds with FS-DNA, the intrinsic binding constant $K_b$ was determined by monitoring the changes in absorbance by using the following equation [59]:

$$\frac{1}{\varepsilon_a-\varepsilon_b} = \frac{1}{\varepsilon_b-\varepsilon_f} + \frac{1}{K_b(\varepsilon_b-\varepsilon_f)[\mathrm{BM}]} \quad (2)$$

where [BM] is the concentration of biomacromolecule while here the [BM] is concentration of FS-DNA; $\varepsilon_a$, $\varepsilon_f$ and $\varepsilon_b$ are the apparent extinction coefficient, the extinction coefficient for free compounds and the extinction coefficient for the compounds in a fully bound form, respectively. $\varepsilon_f$ was determined by calibration curve and $\varepsilon_a$ is the ratio of $A_{obs}$ to [complex]. A plot of $1/(\varepsilon_a - \varepsilon_f)$ versus 1/[DNA] gives $K_b$ as ratio of y-intercept to slope. The binding constants of FS-DNA with Cu(II), Zn(II), Co(II) and Ni(II) complexes were $2.46 \times 10^4$, $2.09 \times 10^4$, $2.03 \times 10^4$, and $9.85 \times 10^3$ $M^{-1}$, respectively.

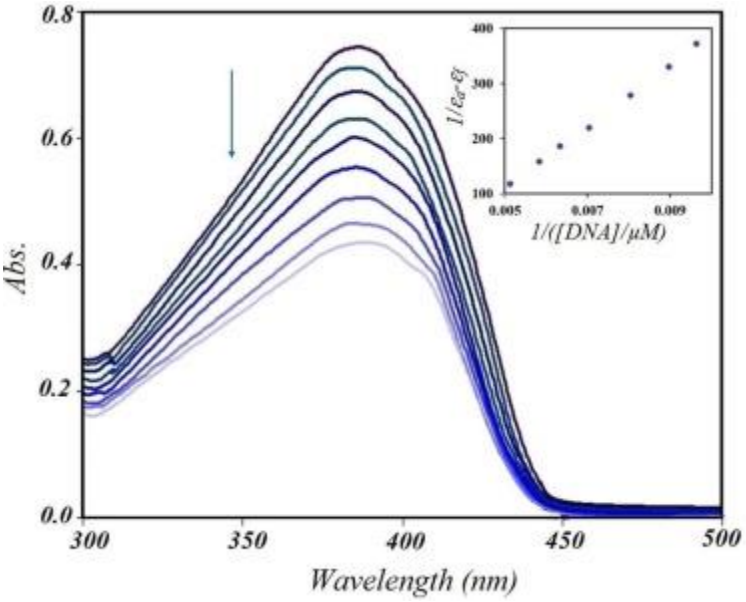


Fig. 7. UV absorption spectra of **NiL2** in the presence of various amounts of DNA. [complex] = $1 \times 10^{-4}$ M, [DNA] = 0–$5 \times 10^{-4}$ M.

### *3.3.2. Fluorescence spectroscopy*

The fluorescence measurements were performed in order to investigate the interaction mode between the synthesized metal complexes and FS-DNA. Ethidium bromide (EtBr) is a standard intercalating agent of DNA that is used to study DNA-binding of compounds. It was known that EtBr has only a weak fluorescence emission in solution, while a significant increase of its fluorescence intensity can be observed when it binds to DNA in view of its strong intercalation between the adjacent base pairs of DNA [60], [61], [62], [63]. The fluorescence quenching of DNA-EtBr with addition of metal complexes are shown in Figs. 8 and S2. Synthesized metal complexes are not able to have efficiently competition with EtBr as strong intercalators due to their non-planer structure. However, these complexes can displace EtBr in a non-competitive manner by changing the DNA conformation. Consequently, the DNA-bound EtBr molecules are converted to their free form in solution and cause fluorescence quenching. In order to determine the binding ability between the compounds and FS-DNA, the Stern–Volmer quenching plot was obtained by monitoring the fluorescence quenching of EtBr-DNA with increasing the concentration of the compounds according to the Stern–Volmer equation [64]:

$$\frac{F_0}{F} = 1 + K_{SV}[Q] = 1 + k_q \tau [Q] \quad (3)$$

where, $F_0$ and $F$ are the fluorescence intensity of EtBr-DNA in absence and presence of the compounds. $K_{SV}$ is the Stern-Volmer quenching constant, $k_q$ is the quenching rate constant of and $\tau$ is the average lifetime without quencher which is typically equal to $10^{-8}$ s for biomacromolecules [65]. The values of $K_{sv}$ for synthesized complexes are determined from the plot of $F_0/F$ vs. [Q] (Figs. 8 and S2) and were presented in Table 4. Fluorescence quenching is classified to two mechanisms including static quenching and dynamic quenching. In the static mechanism, the fluorophore and the quencher collide are both in the ground state while

fluorophore and quencher collide together in the excited state in dynamic mechanism [65]. Linearity of the Stern–Volmer plot indicates that quenching fluorescence has only one mechanism, either dynamic or static [66]. In this study, the values of $k_q$ were about $10^{11}$ $M^{-1}.s^{-1}$ which are greater than the limiting diffusion rate constant of the diffusional quenching for biopolymers ($2 \times 10^{10}$ $M^{-1}.s^{-1}$). This observation supports that quenching fluorescence occurs through static mechanism [65].

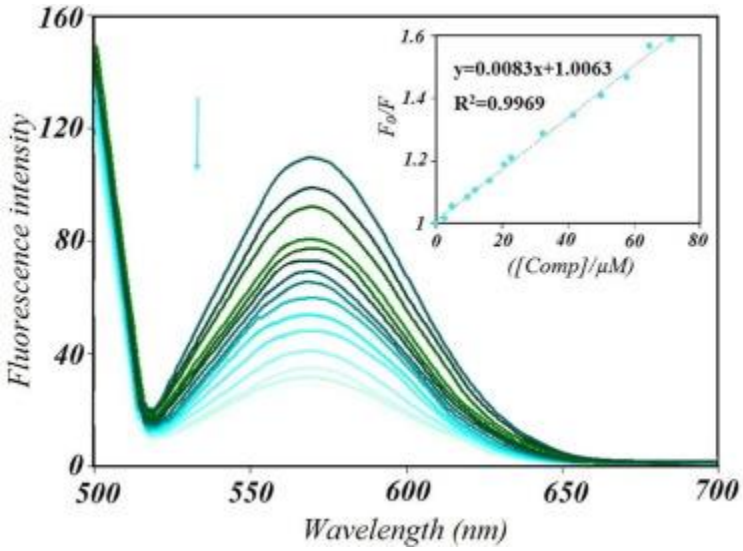


Fig. 8. Fluorescence emission spectra of ethidium bromide-DNA system in the presence of various amounts of **NiL$_2$**. [DNA] = $5 \times 10^{-5}$ M, [EtBr] = $5 \times 10^{-6}$ M, [complex] = 0–$250 \times 10^{-6}$ M.

Table 4. The DNA-binding constant ($K_b$), binding energy, the number of binding site (n) and the Stern-Volmer constant ($K_{SV}$) of the metal complexes.

| Type of Complex | $K_{binding}/M^{-1}$ (Fluorescence) | $K_{binding}/M^{-1}$ (UV–Vis) | Binding Energy/kcal.mol$^{-1}$ (Docking) | n | $K_{sv}/M^{-1}$ |
|---|---|---|---|---|---|
| **CuL$_2$** | 2.46 (±0.14) × $10^4$ | 9.38 (±0.21) × $10^3$ | −7.14 | 0.7354 | 0.69 (±0.03) × |
| **ZnL$_2$** | 2.09 (±0.11) × $10^4$ | 3.51 (±0.17) × $10^3$ | −6.82 | 0.6428 | 0.52 (±0.02) × |
| **CoL$_2$** | 2.03 (±0.03) × $10^4$ | 3.25 (±0.14) × $10^3$ | −6.17 | 0.7159 | 0.56 (±0.04) × |
| **NiL$_2$** | 9.85 (±0.09) × $10^3$ | 3.04 (±0.10) × $10^3$ | −6.11 | 0.9614 | 0.83 (±0.01) × |

Moreover, the binding constant ($K_b$) have been determined by using the following equation [66]:

$$\mathrm{Ln}\left(\frac{F_0 - F}{F}\right) = \mathrm{Ln}(K_b) + n\mathrm{Ln}[Q] \quad (4)$$

where, [Q] is the concentration of quencher that is the synthesized compounds here. "$K_b$" is obtained from the plot of Ln((F0-F)/F) versus Ln[Q] as a y-intercept. Furthermore, "*n*" which is the number of binding site per DNA is slope of the plot (Fig. S5). The value of *n* is nearly 1, indicating that the synthesized complexes bind to DNA with molar ratio of 1:1. The calculated results are shown in Table 4 and are in good agreement with the UV–Vis spectroscopy results.

### *3.3.3. Viscosity measurements*

To further verify of interaction mode between the metal complexes and DNA, viscosity measurements of DNA upon addition of the complexes were carried out. A classical intercalative mode causes an increase in the DNA viscosity. Because of base pairs are separated in order to accommodate the binding ligand and then the overall length of DNA increases [51]. Non-classical mode of interactions such as groove binding and electrostatic could bend the DNA helix, reduces its length and causes the reduction or no change in the DNA viscosity [51]. The effect of the metal complexes on the viscosity of DNA is illustrated in Fig. 9. As can be seen, the viscosity of DNA decreased slightly or remained constant with an increasing amounts of complexes, indicating the binding mode of all complexes may be groove binding. This result is consistent with molecular docking results (Section 3.3.4.).

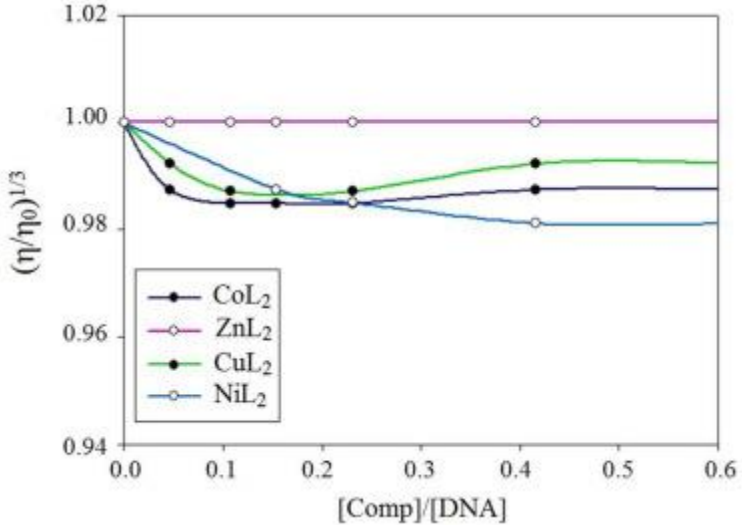


Fig. 9. Effect of increasing amounts of metal complexes on the viscosity of DNA. [Complex] / [DNA] = 0–0.6.

### *3.3.4. Molecular docking*

To obtain a deep insight about DNA binding of complexes, molecular docking studies were carried out. The docked model results suggest that all complexes bind to the minor groove of DNA. Table 5 represents the binding mode and the nucleotides around each of metal complexes. The **$CuL_2$**, **$ZnL_2$**, **$CoL_2$** and **$NiL_2$** complexes formed two, three, one and one hydrogen bond interactions with DNA, respectively. Also, there are two π-π stacking interactions between Cu(II) complex and DG4 nucleotide of DNA. The docking poses of metal complexes-DNA and participant nucleotides in H-bond and π-π stacking interactions are presented in Fig. 10. The standard binding free energies ($\Delta G°$), describing the affinity of the complexes for binding to DNA

with the best scores, are −7.14, −6.82, −6.17 and −6.11 kcal.mol$^{-1}$ for **CuL$_2$**, **ZnL$_2$**, **CoL$_2$** and **NiL$_2$** complexes, respectively. The docking results are in good agreement with spectroscopic results (see Table 4). Both experimental and computational results collectively suggest that Cu(II) complex has more DNA binding affinity than the other synthesized complexes and all of the synthesized complexes are DNA groove binder. The binding of a ligand to the minor groove of DNA simplifies the interaction between ligand and minor groove binding proteins which are needed for gene expression [67].

Table 5. Molecular docking Results for the interaction of metal complexes with DNA.

| **Type of complex** | **Bases around complex** | **Hydrogen bond** | **π-π or π-cation interaction** | **Binding site** | **Zoom in (Conformation of complex in binding site)** |
|---|---|---|---|---|---|
| **CuL$_2$** | DT24- DG23- DC3- DG4- DG22- DA5 | Yes | Yes | 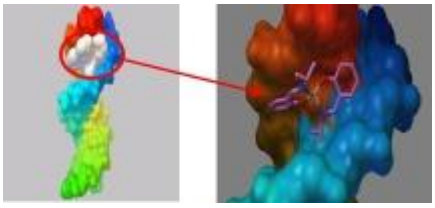 | |
| **ZnL$_2$** | DT12- DG11- DG10- DC15- DG16- DA17 | Yes | No | 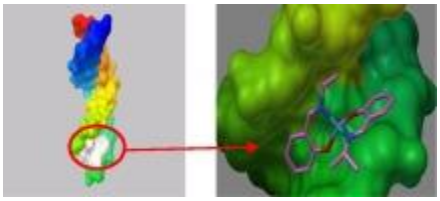 | |
| **CoL$_2$** | DG7- DT8- DC9- DT20- DG19- DC18 | Yes | No | 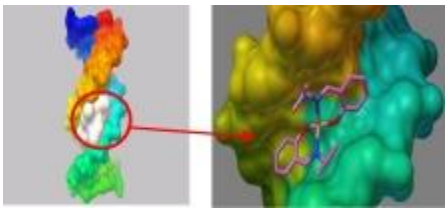 | |
| **NiL$_2$** | DC9- DT8- DC18- DG7- DG19- DT20 | Yes | No | 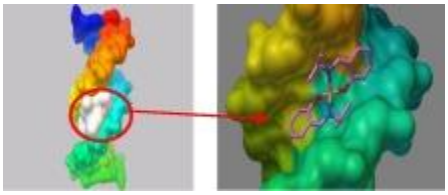 | |

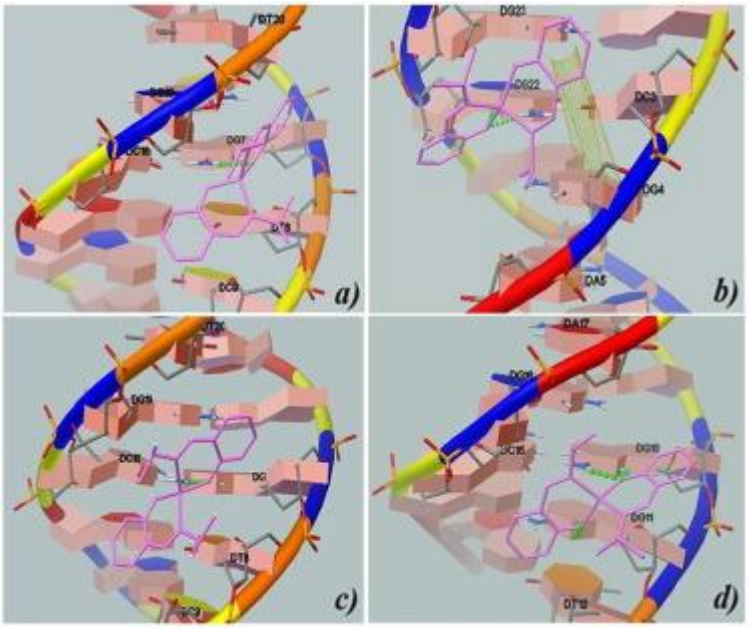


Fig. 10. The docking pose of metal complex-DNA system: a) **CoL$_2$**, b) **CuL$_2$**, c) **NiL$_2$**, d) **ZnL$_2$**. (The small green spheres and yellow cylinders show H-bond interactions and π-π interactions, respectively).

### 3.4. Interaction with human serum albumin (HSA)

Drug-protein interaction affects the drug absorption, distribution and elimination in the cardiovascular system [68]. Moreover, this binding can prevent rapid elimination of drugs from bloodstream [69], and also increase drug solubility in plasma, decrease its toxicity, protect from oxidation and prolong its *in vivo* half-life [70]. The requirement of HSA-binding study in design and synthesis new drugs interested us to investigate HSA-binding behavior of the synthesized metal complexes. Consequently, fluorescence quenching experiment together with chemometrics method have been carried out to obtain information including binding mode, binding constants, number of binding sites and intermolecular distances [71]. The UV–Vis absorption spectroscopy was performed in order to calculate binding constant. More details about binding mode of synthesized metal complexes to HSA were detected by means of molecular docking calculations.

#### *3.4.1. UV–Vis absorption*

UV–Vis absorption spectroscopy is an effective and simple technique to study the HSA-drug binding. The absorption spectra of the complexes in the absence and presence of different concentrations of HSA were given in Figs. 11 and S3. The intensity of these spectra decreased with the addition of HSA. To quantitatively evaluate of complexes affinity with HSA, the intrinsic binding constant $K_b$ was determined by monitoring the changes in absorbance using Eq. (2). The binding constants of HSA with **NiL$_2$**, **ZnL$_2$**, **CuL$_2$** and **CoL$_2$** complexes are determined as $3.72 \times 10^4$, $3.08 \times 10^4$, $9.80 \times 10^3$, and $3.38 \times 10^3$ $M^{-1}$, respectively.

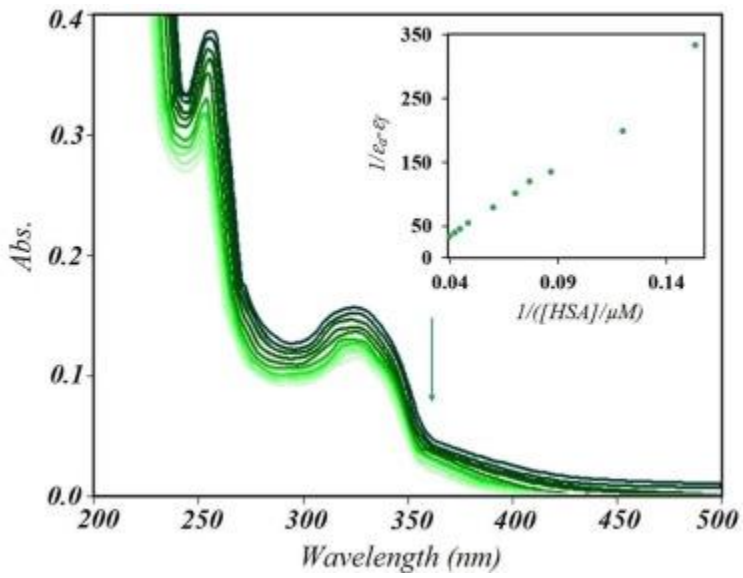


Fig. 11. UV absorption spectra of **NiL$_2$** in the presence of various amounts of HSA. [complex] = $1 \times 10^{-5}$ M, [HSA] = 0–$5 \times 10^{-5}$ M.

### *3.4.2. Fluorescence spectroscopy*

Fluorescence quenching experiment has been performed to investigate the mechanism of interaction between HSA and the compounds. Although the fluorescence of HSA arise from tryptophan (Trp), tyrosine (Tyr), and phenylalanine (Phe) residues, its intrinsic fluorescence is mainly due to tryptophan [72]. The fluorescence intensity of protein was quenched through the addition of complexes. This implies that the compounds strongly interact with HSA, leading to changes of microenvironment around the Trp-214 residue in HSA [70], [73]. Figs. 12 and S4 show the fluorescence quenching of $5 \times 10^{-6}$ M HSA at the presence of various amount of the compounds (0–$5 \times 10^{-5}$ M). It has been found that the fluorescence emission of synthesized metal complexes has considerable overlap with fluorescence emission of HSA. Hence, using $F$ in Eqs. (3) and (4) is an approximation; thus, these equations cannot predict the actual binding constant. In order to overcome to this shortcoming, the chemometrics method was used. This method allows concentration information of an individual component to be extracted in the presence of other constituents. Thus, it is highly useful for solving analytical problems involving a complex matrix. Separation of the experimental results obtained of fluorescence emission into its components was performed by regression analysis using a written program in our laboratory running in the MATLAB 7.2 (The MathWork Co.) environment. Calculations were performed by an iterative procedure by using the Newton–Gauss–Levenberg/Marquardt (NGL/M) algorithm of nonlinear least squares fitting [74].

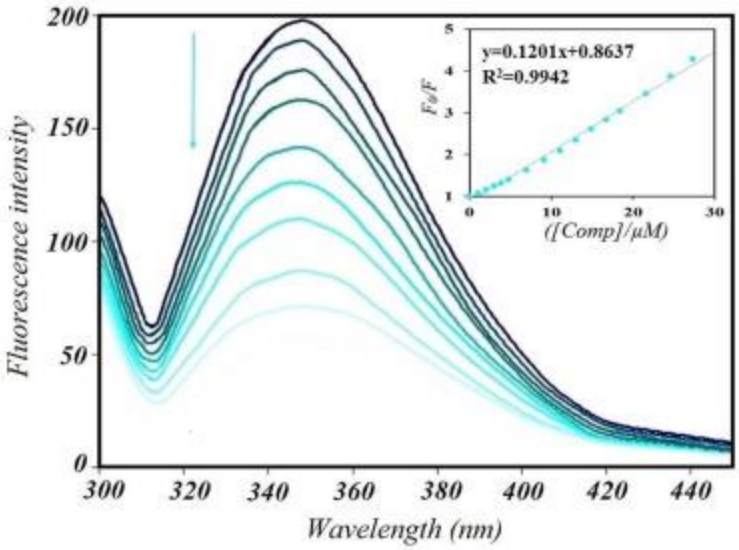


Fig. 12. Quenching in fluorescence spectra of HSA upon its titration with various amounts of **NiL**$_2$. [HSA] = $5 \times 10^{-6}$ M, [complex] = $0–50 \times 10^{-6}$ M.

The data were processed by using the proposed chemical equilibria (model; eg. P + A ↔ AP) and an initial estimate of the binding constant (K) values. The program then minimizes the following equation based on the variation of K in each titration and considers some restrictions such non-negativity in concentration and the fluorescence intensities [75].

$$\sum_{i=0}^{ns} (F_{exp} - F_{calc})_i^2 \cong 0 \qquad (5)$$

where ns is the number of solution (total titration steps) and "exp" and "calc" are referred to recorded and calculated signals, respectively. The output of program comprises the refined parameters (net fluorescence of HSA, metal complex and HSA-metal complex systems), the sum-of-squares and the standard deviation of the binding constant.

The computer fit of the fluorescence-mole ratio data for compounds is shown in Fig. 13.

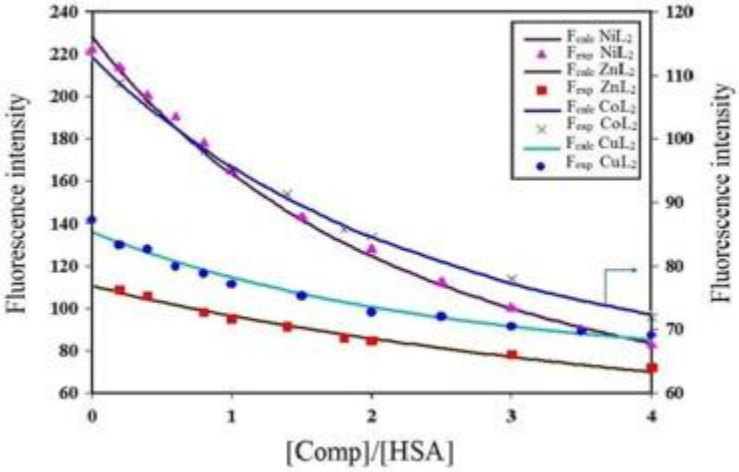

Fig. 13. The computer fit of the fluorescence-mole ratio data for the synthesized metal complexes.

In order to determine the binding ability between the compounds and HSA, the Stern–Volmer quenching plot was obtained by monitoring the net fluorescence quenching of HSA (extracted from chemometrics results) with increasing the concentration of the compounds according to the Stern–Volmer equation (Eq. (3)). The values of $K_{sv}$ for the synthesized complexes are determined from the plot of $F_0/F$ vs. [Q] (Figs. 12 and S4) and were presented in Table 6. Moreover, the obtained values for $k_q$ are about $10^{12}$-$10^{13}$ $M^{-1}.S^{-1}$ that are greater than maximum collision quenching constant ($2 \times 10^{10}$ $M^{-1}.S^{-1}$) of various quenchers with the biomacromolecules. This result represents the existence of static quenching mechanism. The binding constants ($K_b$) of the metal complexes and HSA are calculated using Eq. (4) (Fig. S6) and are presented in Table 6. Comparison between obtained results from fluorescence quenching with UV–Vis absorption showed a good agreement between them and represents high affinity of HSA for all synthesized metal complexes. In general, binding constant of a drug with a carrier protein such as HSA should be high enough to bind and transfer throughout the body. Moreover, in order to release a drug on target, it should not be too high. HSA Binding constants of all the synthesized compounds are in a good range ($2–7 \times 10^4$ $M^{-1}$) [76] and also are comparable to analogue compounds and some potent drugs **(**Table 7**)**.

Table 6. The HSA-binding constant ($K_b$), binding energy, the number of binding site (n) and the Stern-Volmer constant ($K_{SV}$) of the metal complexes.

| Type of Complex | $K_{binding}/M^{-1}$ (Fluorescence) | $K_{binding}/M^{-1}$ (UV–Vis) | Binding Energy/kcal.mol$^{-1}$ (Docking) | n | $K_{sv}/M^{-1}$ |
|---|---|---|---|---|---|
| **$NiL_2$** | 6.84 (±0.18) × $10^4$ | 3.72 (±0.27) × $10^4$ | −6.75 | 1.156 | 1.201 (±0.08) × 10 |
| **$ZnL_2$** | 4.53 (±0.16) × $10^4$ | 3.08 (±0.24) × $10^4$ | −6.72 | 1.081 | 0.653 (±0.02) × 10 |
| **$CuL_2$** | 4.30 (±0.14) × $10^4$ | 9.80 (±0.22) × $10^3$ | −6.61 | 1.105 | 0.649 (±0.02) × 10 |
| **$CoL_2$** | 2.77 (±0.15) × $10^4$ | 3.38 (±0.21) × $10^3$ | −6.04 | 1.064 | 0.373 (±0.07) × 10 |

*Standard Deviation.

Table 7. The value of $K_b$ of some metal complexes and potent drugs.

| Compound | $K_b/M^{-1}$ | Ref. |
|---|---|---|
| $[Pd(obap)]^-$ | 5.56 × $10^4$ | [77] |
| $[Pd(mda)]^{2-}$ | 2.11 × $10^4$ | [77] |

| Compound | $K_b/M^{-1}$ | Ref. |
|---|---|---|
| $PdCl_2$(N,*N*-IM) | $5.29 \times 10^4$ | [78] |
| $Cu(IPA)_2(Phen)$ | $1.13 \times 10^4$ | [64] |
| $[NiL]\cdot CH_3OH$ = NSC | $1.08 \times 10^4$ | [79] |
| $Cu(OAc)_2L_2\cdot 2H_2O$ | $2.67 \times 10^4$ | [80] |
| $Ni(OAc)_2L_2\cdot 2H_2O$ | $2.19 \times 10^4$ | [80] |

Furthermore, these synthesized complexes are uncharged which and this is an advantage for a drug. Several researches show that the unionized drugs are soluble in lipid and capable of crossing through the membrane's lipid bilayer while the ionized analogue species fail to cross [81].

### *3.4.3. Energy transfer from HSA to complexes*

Energy transfer between the compounds and HSA can provides valuable information about HSA-complex binding. The fluorescence quenching of HSA upon its binding to metal complex can be indicative of energy transfer between HSA and metal complex. This energy transfer can be explained by fluorescence resonance energy transfer (FRET) theory. FRET also known as Förster's resonance energy transfer which is an interaction between the excited molecule and its adjacent molecule. Upon this interaction, energy absorbed by donor molecule is transferred to an acceptor [82]. According to this theory, three conditions are required to energy transfer: (1) the donor should have fluorescence, (2) the fluorescence emission spectrum of the donor and the UV–Vis spectrum of the acceptor should have sufficient overlap (3) a small distance between donor and acceptor (<8 nm) [82]. The distance and efficiency of energy transfer (*E*) between tryptophan residue of protein (HSA) and drug (complex) has been calculated by using this theory through the following equation:

$$\mathrm{E} = 1 - \frac{\mathrm{F}}{\mathrm{F_0}} = \frac{\mathrm{R_0^6}}{\mathrm{R_n^6 + r^6}} \tag{6}$$

where $R_0$ is the critical distance when the transfer efficiency is 50%; $r$ is the distance between donor and acceptor. $R_0$ can be calculated by Eq. (7) [83].

$$\mathrm{R_0^6} = 8 \cdot 79 \times 10^{-25} \mathrm{K^2 N^{-4} J}\varphi \tag{7}$$

In the above equation, the term $K^2$ is the orientation factor of the dipoles; $N$ is the refracted index of medium, $J$ is the overlap integral of the fluorescence spectrum of the donor with absorption spectrum of the acceptor and $\varphi$ is the fluorescence quantum yield of the donor. The value of $J$ can be calculated by the following expression:

$$\mathrm{J} = \frac{\sum \mathrm{F}(\lambda)\varepsilon(\lambda)\lambda^4 \Delta\lambda}{\sum \mathrm{F}(\lambda)\Delta\lambda} \tag{8}$$

where, $F(\lambda)$ is the fluorescence intensity of the donor in the absence of the acceptor at wavelength $\lambda$ and $\varepsilon$ is the molar absorption coefficient of the acceptor at $\lambda$. In the present case, $K^2 = 2/3$, $N = 1.336$ and $\varphi = 0.15$ for HSA. The parameters for the synthesized compounds were calculated according to Eqs. (6), (7), (8) (Table 8). Fig. 14 represents the overlap of the fluorescence emission spectrum and the UV–Vis spectrum of HSA-**ML₂** complexes with 1:1 M ratio of HSA to **ML₂**. The values of $r$ for all the compounds are less than 8 nm and $0.5\ R_0 < r < 1.5\ R_0$, suggesting that energy transfer from HSA to metal complexes occurs with high probability.

Table 8. The obtained results from FRET theory for the metal complexes.

| Type of Complex | $R_0$(nm) | r(nm) | E |
|---|---|---|---|
| **$NiL_2$** | 0.40 | 0.40 | 0.48 |
| **$ZnL_2$** | 1.32 | 1.28 | 0.55 |
| **$CuL_2$** | 0.32 | 0.34 | 0.43 |
| **$CoL_2$** | 0.29 | 0.29 | 0.50 |

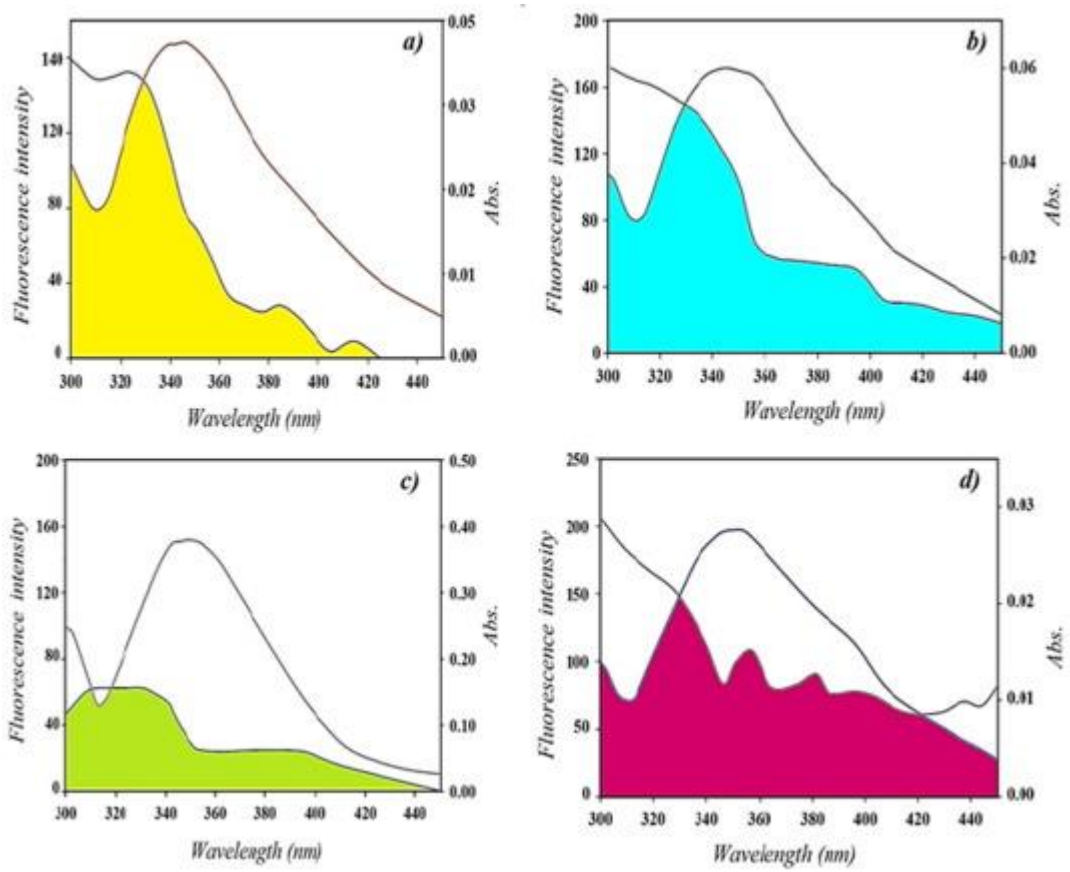


Fig. 14. Overlap of the fluorescence spectra and the UV absorption spectra of HSA-metal complex systems: a) **$CoL_2$**, b) **$CuL_2$**, c) **$NiL_2$**, d) **$ZnL_2$**.

### *3.4.4. Molecular docking of the metal complexes with HSA*

In this work, the **$CuL_2$**, **$CoL_2$**, **$NiL_2$** and **$ZnL_2$** complexes were docked to the crystal structure of HSA. The molecular docking results showed that all synthesized metal complexes are bound to the boundary of IIA-IIB subdomains which is the main binding site for some drugs such as diflunisal, ibuprofen and halothane (Table 9). The results indicated that H-bond interactions, hydrophobic interactions, π-π stacking and π-cation interactions have a dominant role in the stability of **$CuL_2$**, **$ZnL_2$** and **$NiL_2$** complexes-HSA. While, there is no H-bond interactions, π-π stacking or π-cation interactions in the **$CoL_2$**-HSA complex. The docking poses of all metal complexes-HSA are shown in Fig. 15. The binding energy for **$NiL_2$**, **$ZnL_2$**, **$CuL_2$** and **$CoL_2$** complexes are evaluated about -6.75, -6.72, -6.61 and -6.04 kcal.mol$^{-1}$, respectively. The larger negative value of binding energy for Ni(II) complex means the higher affinity for HSA binding which is in good agreement with UV–Vis and fluorescence experimental data. Additionally, the distances between Trp-214 and metal complexes were 0.39, 0.32, 0.39 and 0.44 nm for **$NiL_2$**, **$ZnL_2$**, **$CuL_2$** and **$CoL_2$** complexes, respectively. These values are in consistent with obtained r values from FRET calculations.

Table 9. Molecular docking Results for the interaction of metal complexes with HSA.

| Type of complex | Hydrophilic amino acids around complex | Hydrophobic amino acids around complex | Binding Site | Zoom in (Conformation of complex in binding site) |
|---|---|---|---|---|
| **$NiL_2$** | TRP214-LYS199-GLN196-ARG257-LYS195-ARG218-ARG222 | LEU219-ALA291-LEU238 | | 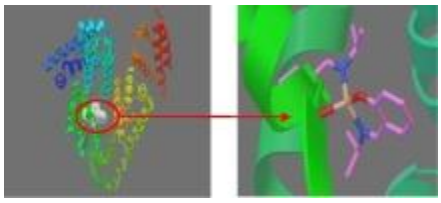 |
| **$ZnL_2$** | TRP214-LYS199-GLU292-ARG222-LYS195-GLN196 | LEU238-LEU198-VAL455-ALA291 | | 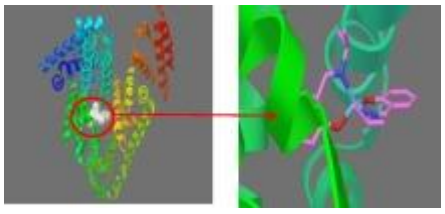 |
| **$CuL_2$** | LYS199-GLN196-LYS195-TYR150-ARG257-GLU292-ARG222 | LEU198-VAL455-ALA291 | | 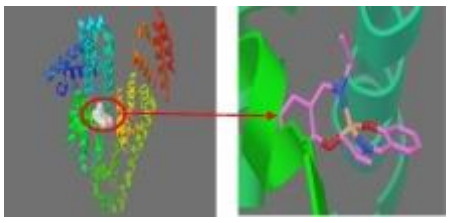 |

| Type of complex | Hydrophilic amino acids around complex | | Hydrophobic amino acids around complex | | Binding Site | Zoom in (Conformation of complex in binding site) |
|---|---|---|---|---|---|---|
| **$CoL_2$** | SER480-<br>LYS351 | ARG209- | PHE206-<br>VAL482-<br>ALA213-<br>ALA350 | LEU481-<br>ALA210-<br>LEU347- | 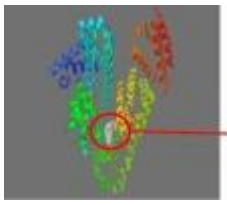 | 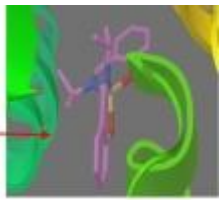 |

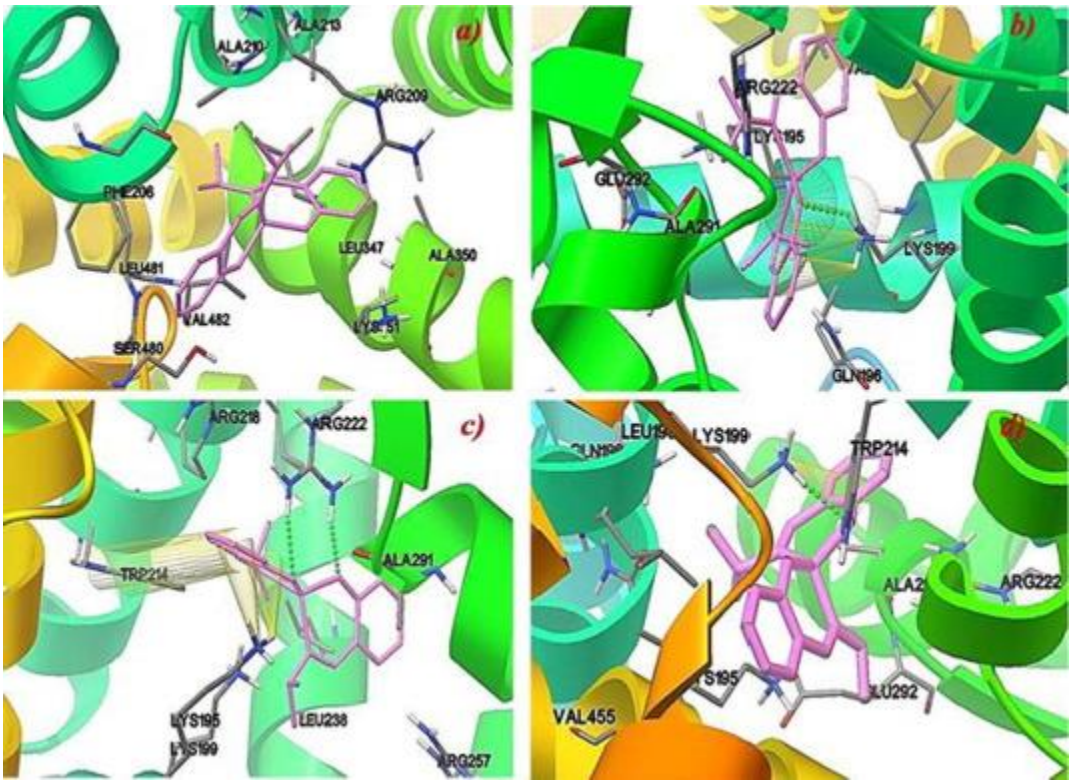


Fig. 15. The docking pose of metal complex-HSA systems: a) **$CoL_2$**, b) **$CuL_2$**, c) **$NiL_2$**, d) **$ZnL_2$**. (Small green spheres, yellow cylinders and yellow cones show H-bond interactions, π-π interactions and π-cation interactions, respectively.)

## 4. Conclusion

In conclusion, we have synthesized four new Schiff base complexes, **$NiL_2$**, **$CoL_2$**, **$CuL_2$** and **$ZnL_2$**, derived from a bidentate Schiff-base ligand (**HL**: ((E)-2-((isopropylamino)methyl)phenol). The structures of all complexes have been established by single crystal X-ray diffraction. The crystallographic data reveal that in all the complexes the metal centers are four-coordinated by two phenolic-O atoms and two azomethine-N atoms to form a distorted tetrahedral geometry. The DNA- and HSA-binding of the synthesized metal complexes

were investigated by using both experimental (fluorescence quenching, viscosity measurements and UV–Vis spectroscopy) and computational methods (chemometrics and molecular docking). Chemometrics method was carried out in order to study HSA-binding of complexes, quantitively. The obtained HSA-binding constant values from experimental and computational methods stated that the Ni(II) complex-HSA is more stable than the others. Molecular docking studies showed that H-bond interactions, hydrophobic interactions, π-π stacking and π-cation interactions have a dominant role in the stability of complex-HSA. The computational docking and viscosity data suggest that all metal complexes interact with DNA by the groove binding mechanism. The results showed that Cu(II) complex exhibited stronger DNA binding affinity than other complexes.

Acknowledgement
The authors are grateful to the Research Council of the University of Isfahan for financial support of this work.

Appendix A. Supplementary data
CCDC 1487336, 1487337, 1487338 and 1487339 contain the supplementary crystallographic data for NiL2, CoL2, CuL2, and ZnL2, respectively. These data can be obtained free of charge via http://dx.doi.org/10.1016/j.ica.2017.05.035, or from the Cambridge Crystallographic Data Centre, 12 Union Road, Cambridge CB2 1EZ, UK. Fax: +44 1223 336 033; or e-mail: deposit@ccdc.cam.ac.uk. Supplementary data associated with this article can be found, in the online version, at http://dx.doi.org/10.1016/j.ica.2017.05.035.

References

[1] L. Ronconi, P. Sadler, J. Coord. Chem. Rev. 251 (2007) 1633.
[2] M.L. Low, L. Maigre, P. Dorlet, R. Guillot, J.M. Pagès, K.A. Crouse, C. Policar, N. Delsuc, Bioconjugate Chem. 25 (2014) 2269.
[3] X. Wang, J. Yin, L. Shi, G. Zhang, B. Song, Eur. J. Med. Chem. 77 (2014) 65.
[4] L.A. Saghatforoush, F. Chalabian, A. Aminkhani, G. Karimnezhad, S. Ershad, Eur. J. Med. Chem. 44 (2009) 4490.
[5] A.M. Asiri, S.A. Khan, H.M. Marwani, K. Sharma, J. Photochem. Photobiol., B 120 (2013) 82.
[6] P. Noblia, M. Vieites, B.S. Parajon-Costa, E.J. Baran, H. Cerecetto, P. Draper, M. Gonzalez, O.E. Piro, E.E. Castellano, A. Azqueta, A.L. Cerain, A. Monge-Vega, D. Gambino, J. Inorg. Biochem. 99 (2005) 443.
[7] L.M.F. Gomes, R.P. Vieira, M.R. Jones, M.C.P. Wang, C. Dyrager, E.M. Souza-Fagundes, J.G. Da Silva, T. Storr, H. Beraldo, J. Inorg. Biochem. 139 (2014) 106.
[8] G. Prakash, R. Manikandan, P. Viswanathamurthi, K. Velmurugan, R. Nandhakumar, J. Photochem. Photobiol., B 138 (2014) 63.
[9] B.K. Seth, A. Ray, A. Saha, P. Saha, S. Basu, J. Photochem. Photobiol., B 132 (2014) 72.
[10] M. Soltani, M. Homayouni-Tabrizi, S. Afsharnezhad, S.A. Beyramabadi, M. Khashi, J. Cell. Immunother. 1 (2015) 18.
[11] C. Liang, J. Xia, D. Lei, X. Li, Q. Yao, J. Gao, Eur. J. Med. Chem. 74 (2014) 742.
[12] X. Qiao, Z.-Y. Ma, C.-Z. Xie, F. Xue, Y.-W. Zhang, J.-Y. Xu, Z.-Y. Qiang, J.-S. Lou, G.-J. Chen, S.-P. Yan, J. Inorg. Biochem. 105 (2011) 728.

[13] X. Zhong, J. Yi, J. Sun, H.-L. Wei, W.-S. Liu, K.-B. Yu, Eur. J. Med. Chem. 41 (2006) 1090.
[14] Y. Mohini, R.B.N. Prasad, M.S.L. Karuna, Y. Poornachandra, C. Ganesh Kumar, Bioorg. Med. Chem. Lett. 24 (2014) 5224.
[15] Y. Jia, J. Li, Chem. Rev. 115 (2015) 1597.
[16] M. Shabbir, Z. Akhter, I. Ahmad, S. Ahmed, H. Ismail, B. Mirza, V. McKee, M. Bolte, J. Mol. Struct. 1116 (2016) 84.
[17] C.T. Prabhakara, S.A. Patil, S.S. Toragalmath, S.M. Kinnal, P.S. Badami, J. Photochem. Photobiol., B 157 (2016) 1.
[18] C.E. Satheesh, P.R. Kumar, P. Sharma, K. Lingaraju, B.S. Palakshamurthy, H.R. Naika, Inorg. Chim. Acta 442 (2016) 1.
[19] M. Yıldız, Ö. Karpuz, C.T. Zeyrek, B. Boyacıog˘lu, H. Dal, N. Demir, N. Yıldırım, H. Ünver, J. Mol. Struct. 1094 (2015) 148.
[20] R. Ramesh, M. Sivagamasundari, Synth. React. Inorg. Met.-Org. Chem. 33 (2003) 899.
[21] X.-Q. Zhou, Y. Li, D.-Y. Zhang, Y. Nie, Z.-J. Li, W. Gu, X. Liu, J.-L. Tian, S.-P. Yan, Eur. J. Med. Chem. 114 (2016) 244.
[22] P.R. Reddy, S. Rajeshwar, B. Satyanarayana, J. Photochem. Photobiol., B 160 (2016) 217.
[23] S. Saha, S. Jana, S. Gupta, A. Ghosh, H.P. Nayek, Polyhedron 107 (2016) 183.
[24] J. Adhikary, P. Kundu, S. Dasgupta, S. Mukherjee, S. Chattopadhyay, G. Aullón, D. Das, Polyhedron 101 (2015) 93.
[25] C. Jing, C. Wang, K. Yan, K. Zhao, G. Sheng, D. Qu, F. Niu, H. Zhu, Z. You, Bioorgan. Med. Chem. 24 (2016) 270.
[26] Z. Kazemi, H. Amiri Rudbari, V. Mirkhani, M. Sahihi, M. Moghadam, S. Tangestaninejad, I. Mohammadpoor-Baltork, J. Mol. Struct. 1096 (2015) 110.
[27] M.C. Heffern, V. Reichova, J.L. Coomes, A.S. Harney, E.A. Bajema, T.J. Meade, Inorg. Chem. 54 (2015) 9066.
[28] S. Adsule, V. Barve, D. Chen, F. Ahmed, Q.P. Dou, S. Padhye, F.H. Sarkar, J. Med. Chem. 49 (2006) 7242.
[29] L.H. Abdel-Rahman, A.M. Abu-Dief, E.F. Newair, S.K. Hamdan, J. Photochem. Photobiol., B 160 (2016) 18.
[30] S. Menati, H. Amiri Rudbari, M. Khorshidifard, F. Jalilian, J. Mol. Struct. 1103 (2016) 94.
[31] I. Khosravi, F. Hosseini, M. Khorshidifard, M. Sahihi, H. Amiri Rudbari, J. Mol. Struct. 1119 (2016) 373.
[32] M. Khorshidifard, H. Amiri Rudbari, B. Askari, M. Sahihi, M. Riahi Farsani, F. Jalilian, G. Bruno, Polyhedron 95 (2015) 1.
[33] H. Amiri Rudbari, M. Khorshidifard, B. Askari, N. Habibi, G. Bruno, Polyhedron 100 (2015) 180.
[34] M. Khorshidifard, H. Amiri Rudbari, Z. Kazemi-Delikani, V. Mirkhani, R. Azadbakht, J. Mol. Struct. 1081 (2015) 494.
[35] H. Keypour, A. Shooshtari, M. Rezaeivala, M. Bayat, H. Amiri Rudbari, Inorg. Chim. Acta 440 (2016) 139.
[36] Z. Kazemi, H. Amiri Rudbari, M. Sahihi, V. Mirkhani, M. Moghadam, S. Tangestaninejad, I. Mohammadpoor-Baltork, S. Gharaghani, J. Photochem.

Photobiol., B 162 (2016) 448.
[37] H. Amiri Rudbari, M.R. Iravani, V. Moazam, B. Askari, M. Khorshidifard, N. Habibi, G. Bruno, J. Mol. Struct. 1125 (2016) 113–120.
[38] H. Iranmanesh, M. Behzad, G. Bruno, H. Amiri Rudbari, H. Nazari, A. Mohammadi, O. Taheri, Inorg. Chim. Acta 395 (2013) 81.
[39] M. Pooyan, A. Ghaffari, M. Behzad, H. Amiri Rudbari, G. Bruno, J. Coord. Chem. 66 (2013) 4255.
[40] A. Ghaffari, M. Behzad, M. Pooyan, H. Amiri Rudbari, G. Bruno, J. Mol. Struct. 1063 (2014) 1.
[41] H. Keypour, M. Shayesteh, D. Nematollahi, L. Valencia, H. Amiri Rudbari, J. Coord. Chem. 63 (2010) 165.
[42] G. Grivani, M. Vakili, A.D. Khalaji, G. Bruno, H. Amiri Rudbari, M. Taghavi, V. Tahmasebi, J. Mol. Struct. 1072 (2014) 77.
[43] G. Grivani, G. Bruno, H. Amiri Rudbari, A.D. Khalaji, P. Pourteimouri, Inorg. Chem. Commun. 18 (2012) 15.
[44] H. Keypour, R. Azadbakht, H. Amiri Rudbari, A. Heydarinekoo, H.R. Khavasi, Trans. Met. Chem. 34 (2009) 835.
[45] H. Amiri Rudbari, M. Riahi Farsani, S. Lanza, G. Bruno, B. Yadollahi, C. R. Chim. 18 (2015) 391.
[46] (a) COSMO, version 1.60, Bruker AXS Inc., Madison, Wisconsin, 2005.;
(b) SAINT, version 7.06A, Bruker AXS Inc., Madison, Wisconsin, 2005.;
(c) SADABS, version 2.10, Bruker AXS Inc., Madison, Wisconsin, 2005.
[47] M.C. Burla, R. Caliandro, M. Camalli, B. Carrozzini, G.L. Cascarano, L. De Caro, C. Giacovazzo, G. Polidori, R. Spagna, J. Appl. Crystallogr. 38 (2005) 381.
[48] G.M. Sheldrick, SHELXL-97, University of Göttingen, Göttingen, Germany, 1997.
[49] O.V. Dolomanov, L.J. Bourhis, R.J. Gildea, J.A.K. Howard, H. Puschmann, J. Appl. Crystallogr. 42 (2009) 339.
[50] M.E. Reichmann, S.A. Rice, C.A. Thomas, P. Doty, J. Am. Chem. Soc. 76 (1954) 3047.
[51] Z. Kazemi, H. Amiri Rudbari, M. Sahihi, V. Mirkhani, M. Moghadam, S. Tangestaninejad, I. Mohammadpoor-Baltork, G. Azimi, S. Gharaghani, A. Abbasi Kajani, J. Photochem. Photobiol., B 163 (2016) 246.
[52] F. Ding, L. Zhang, J.X. Diao, X.N. Li, L. Ma, Y. Sun, Ecotox. Environ. Saf. 79 (2012) 238.
[53] A.V. Fonin, A.I. Sulatskaya, I.M. Kuznetsova, K.K. Turoverov, PLoS One 9 (2014) 103878.
[54] C.N. Pace, F. Vajdos, L. Fee, G. Grimsley, T. Gray, Protein Sci. 4 (1995) 2411.
[55] G.M. Morris, D.S. Goodsell, R.S. Halliday, R. Huey, W.E. Hart, R.K. Belew, A.J. Olson, J. Comput. Chem. 19 (1998) 1639.
[56] K. Zheng, F. Liu, X.-M. Xu, Y.-T. Li, Z.-Y. Wu, C.-W. Yan, New J. Chem. 38 (2014) 2964.
[57] M. Sirajuddin, S. Ali, A. Badshah, J. Photochem. Photobiol., B 124 (2013) 1.
[58] K. Abdi, H. Hadadzadeh, M. Weil, H. Amiri Rudbari, Inorg. Chim. Acta 416 (2014) 109.
[59] S.S. Bhat, A.A. Kumbhar, H. Heptullah, A.A. Khan, V.V. Gobre, S.P. Gejji, V.G.

Puranik, Inorg. Chem. 50 (2010) 545.
[60] F. Arjmand, A. Jamsheera, D.K. Mohapatra, J. Photochem. Photobiol., B 121 (2013) 75.
[61] X.B. Fu, G.T. Weng, D.D. Liu, X.Y. Le, J. Photochem. Photobiol., A 276 (2014) 83.
[62] M.J. Waring, J. Mol. Biol. 13 (1965) 269.
[63] P. Fromherz, B. Rieger, J. Am. Chem. Soc. 108 (1986) 5361.
[64] S.U. Dighe, S. Khan, I. Soni, P. Jain, S. Shukla, R. Yadav, P. Sen, S.M. Meeran, S. Batra, J. Med. Chem. 58 (2015) 3485.
[65] F. Darabi, H. Hadadzadeh, M. Ebrahimi, T. Khayamian, H. Amiri, Inorg. Chim. Acta 409 (2014) 379.
[66] S.U. Dighe, S. Khan, I. Soni, P. Jain, S. Shukla, R. Yadav, P. Sen, S.M. Meeran, S. Batra, J. Med. Chem. 58 (8) (2015) 3485–3499.
[67] L.H. Fornander, L. Wu, M. Billeter, P. Lincoln, B. Nordén, J. Phys. Chem. B. 117 (2013) 5820.
[68] F. Li, M. Feterl, J.M. Warner, A.I. Day, F.R. Keene, J.G. Collins, Dalton Trans. 42 (2013) 8868.
[69] B. Demoro, R.F. de Almeida, F. Marques, C.P. Matos, L. Otero, J.C. Pessoa, I. Santos, A. Rodríguez, V. Moreno, J. Lorenzo, Dalton Trans. 42 (2013) 7131.
[70] E.M. Mrkalic´ , R.M. Jelic´ , O.R. Klisuric´ , Z.D. Matovic´ , Dalton Trans. 43 (2014) 15126.
[71] X.-B. Fu, D.-D. Liu, Y. Lin, W. Hu, Z.-W. Mao, X.-Y. Le, Dalton Trans. 43 (2014) 8721.
[72] M. Ganeshpandian, R. Loganathan, E. Suresh, A. Riyasdeen, M.A. Akbarsha, M. Palaniandavar, Dalton Trans. 43 (2014) 1203.
[73] Y.-Q. Wang, H.-M. Zhang, G.-C. Zhang, W.-H. Tao, S.-H. Tang, J. Lumin. 126 (2007) 211.
[74] D.W. Marquardt, J. Sot. Ind. Appl. Math. 11 (1963) 431.
[75] M. Maeder, N. Yorck-Michael, Practical Data Analysis in Chemistry, Elsevier Science, 2006.
[76] M. Kyropoulou, C.P. Raptopoulou, V. Psycharis, G. Psomas, Polyhedron 61 (2013) 126.
[77] J.W. Lown, A.V. Joshua, Biochem. Pharmacol. 28 (1979) 2017.
[78] M. Carreira, R. Calvo-Sanjuán, M. Sanaú, X. Zhao, R.S. Magliozzo, I. Marzo, M. Contel, J. Inorg. Biochem. 116 (2012) 204.
[79] A. Ray, B.K. Seth, U. Pal, S. Basu, Spectrochim Acta A 92 (2012) 164.
[80] S.S. Wu, W.B. Yuan, H.Y. Wang, Q. Zhang, M. Liu, K.B. Yu, J. Inorg. Biochem. 102 (2008) 2026.
[81] O.K. Abou-Zied, PCCP 14 (2012) 2832.
[82] N. Fani, A. Bordbar, Y. Ghayeb, Spectrochim Acta A 103 (2013) 11.
[83] Y. Huang, S. Wang, Y. Bi, J. Jin, M.F. Ehsan, M. Fu, T. He, RSC Adv. 5 (2015) 33254